IUST
Iran University of Science and Technology

Iranian Journal of Electrical and Electronic Engineering

Journal Homepage: ijeee.iust.ac.ir

Research Paper

CFL Stability Conditions for the FDTD Method in Bounded Inhomogeneous Anisotropic Media

K. Hosseini*(C.A.)

Abstract: Anisotropic media appear regularly in electromagnetic wave engineering. The finite-difference time-domain (FDTD) method is a robust technique to model such media. However, the value of the time step in the FDTD algorithm is bounded by the Courant-Friedrichs-Lewy (CFL) condition. In this paper, a simple analytical approach is developed using the Gershgorin circle theorem to derive a point-wise closed-form relation for the CFL condition in bounded inhomogeneous anisotropic media. The proposed technique includes objects of arbitrary shapes with straight, tilted, or curved interfaces located in a computational space with uniform or adaptive gridding schemes. Both axial and non-axial anisotropies are considered in the analysis. The proposed method is able to investigate the effect of boundaries and interfaces on the stability of the algorithm. It is shown that in the presence of an interface between two anisotropic media, the von-Neumann criterion is not able to predict the stability bound for specific ranges of the permittivity tensor components and unit cell aspect ratios. Exploiting the proposed closed-form formulations, it is possible to tune the CFL time step and avoid the temporal instability by the wise selection of the gridding scheme especially in curved boundaries where subcell modelings such as Yu-Mittra formalism are applicable. Some illustrative examples are provided to verify the method by comparing the results with those of the eigenvalue analysis and time-domain simulations.

Keywords: Anisotropic Media, Curved Boundaries, Finite Difference Time Domain (FDTD) Method, Gershgorin Circle Theorem, Inhomogeneous Media, Stability.

1 Introduction

ANISOTROPIC media appear in both microwave and optical structures [1-3]. They are exploited in microstrip lines [4], impedance surfaces [5], holey fibers [6], antennas [7], absorbers [8], and much more applications. Modeling the electromagnetic wave propagation in anisotropic media lacking canonical shapes is challenging because in an anisotropic material the permittivity/permeability is a tensor and hence the field vectors and the flux densities are not aligned. One of the most robust techniques to model wave propagation in complex media is the finite difference time domain (FDTD) method [9], which has been applied to anisotropic media as well. Modeling the anisotropy in the FDTD algorithm requires a specific spatial field interpolation to associate the non-aligned field vectors [10].

One of the challenges of the FDTD method is its temporal instability. The well-known von-Neumann criterion determines the upper stability bound on the FDTD time step in unbounded isotropic media using a spectral domain technique [11]. Consider a two-dimensional computational space filled by an isotropic medium, and discretized into unit cells of sizes $\Delta x \times \Delta y$. Then, the von-Neumann analysis yields

$$\Delta t \le \frac{\sqrt{\varepsilon\mu}}{\sqrt{\frac{1}{\Delta x^2}+\frac{1}{\Delta y^2}}} = \Delta t_{CFL}, \tag{1}$$

Iranian Journal of Electrical and Electronic Engineering, 2022.
Paper first received 19 January 2022, revised 11 February 2022, and accepted 19 February 2022.
* The author is with the Department of Electrical Engineering, Faculty of Engineering, University of Kurdistan, Sanandaj, Kurdistan, Iran.
E-mail: k.hosseini@uok.ac.ir.
Corresponding Author: K. Hosseini.
https://doi.org/10.22068/IJEEE.18.2.2398

which is called the Courant-Friedrichs-Lewy (CFL) condition in unbounded isotropic media [11]. The parameters ε and μ are the electric permittivity and magnetic permeability of the medium, respectively. If the time step exceeds that of (1) the temporal instability will emerge. Although unconditionally stable FDTD methods do not suffer from the CFL limit, the numerical dispersion increases remarkably with the time step [12, 13], and hence in many practical applications where the accuracy cannot be compromised for efficiency, the conventional leapfrog FDTD algorithm is preferred.

There are some reports on the stability analysis of the FDTD in unbounded isotropic dispersive and lossy media using von-Neumann and Routh-Hurwitz techniques [14-18]. However, there are few works dealing with the effect of boundaries and interfaces on the CFL condition. The common practice in studying the FDTD stability in bounded media is to derive the iteration matrix, that associates the fields at two consecutive time steps, and then to calculate the eigenvalues of the matrix [19]. If they lie on/inside the unit circle the algorithm is stable. However, the size of the iteration matrix increases tremendously with the FDTD grid size, and the derivation of the eigenvalues in practical large-scale grids becomes prohibitive. Reference [20], inspired by the theory of dynamical systems, studies the CFL condition in a PEC-enclosed space including nonlinear circuit elements using the concept of numerical energy. However, the effect of interfaces between the media on stability is not investigated. In addition, the CFL time step is derived from a cumulative addition of the elemental energies over the space, and hence the method is not able to find the point which has the most restrictive effect on the stability. In [21] a state-space-based approach is utilized to determine the maximum allowed time step in an inhomogeneous medium and it is shown that the derived time step for a finite medium is less stringent than the CFL condition of the corresponding unbounded medium. This is performed by deriving a closed-form relation for the singular values of a tridiagonal matrix. However, the approach cannot be generalized to anisotropic media. In [22] the CFL condition is investigated in the presence of two one-dimensional elastodynamic media using Gershgorin circle theorem. It is shown that for some ranges of the elastic material properties the CFL limit imposed by the interface is more restrictive than those of the surrounding media. Following [22], we applied the Gershgorin theorem for the first time to the electromagnetic wave propagation at the interface between two one-dimensional simple dielectrics in [23]. Furthermore, we studied the effect of PEC, PMC, and PEMC boundaries on the stability bound of the FDTD method in the free space using a Fourier-based spectral domain technique. Utilizing the Gershgorin theorem, [24] extends the work in [23] to study the stability problem in the two-dimensional free space with a graphene sheet imported to the domain. In both [23] and [24] it is observed that the interfaces and boundaries introduce no further restriction to the CFL condition of the surrounding media.

Some contributions have addressed the problem of stability in the presence of anisotropic media. There is a report which utilizes dual lattices in an anisotropic space to construct a reciprocal conformal FDTD algorithm [25]. This in turn will avoid the late-time instabilities if the time step is chosen within the permitted range. In [26] two overlapped schemes are used to stabilize the algorithm topologically, and the stability analysis is performed via numerical calculation of the eigenvalues of the iteration matrix. In that work, the topological instability is avoided by suppressing the interpolations and extrapolations at the interfaces, and the temporal instability is not studied. In [27] reciprocal interpolation of non-aligned field components is utilized to avoid late-time instability. In [28], a complex ω-plane analysis is carried out to check the causality and hence the dynamic stability of anisotropic PMLs. It is shown that the Cartesian PMLs do not allow dynamic instability. However, at cylindrical and spherical PMLs instability may arise. Up to the author's knowledge, in all works dealing with the stability of the FDTD method in anisotropic media, no closed-form derivation exists for the CFL limit, and the maximum permitted time step is determined numerically.

The contribution of this paper is the derivation of a closed-form CFL time step in a generic inhomogeneous axial or non-axial anisotropic medium of arbitrary shape in an FDTD grid which can use an adaptive meshing scheme. The upper bound is derived point by point and hence it is able to find the points or portions of the space which are responsible for any possible instability. In Section 3, using the Gershgorin circle theorem, the permitted range for the eigenvalues of the iteration matrix of the FDTD algorithm is determined. Then a sufficient upper bound imposed on the time step is derived in an axial anisotropic medium. The derivation is performed for a homogeneous anisotropic medium, two homogeneous anisotropic media with a flat interface, and a generic inhomogeneous anisotropic medium with an arbitrary permittivity profile. In Section 3 the proposed theory is generalized to the non-axial anisotropic media. In Section 4 the eigenvalue analysis of the iteration matrix and time-domain simulations are conducted to validate the proposed theory. Among the simulations, the stability behaviors of homogeneous and inhomogeneous anisotropic cylinders whose boundaries are approximated by staircasing and Yu-Mittra formalism are investigated. Finally, in Section 5 the conclusions are provided.

2 The Proposed Method

A two-dimensional computational space for the TE mode is depicted in Fig. 1, where the field components are restricted to E_x, E_y, and H_z. The space is enclosed by

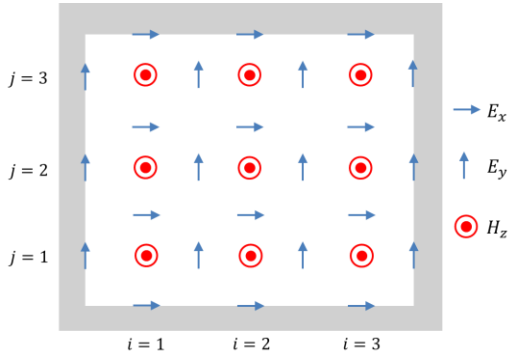

Fig. 1 The TE computational space enclosed by a PEC boundary and filled with an anisotropic medium.

a PEC boundary and is filled with a passive lossless electric-anisotropic medium. Assume that the medium is an axial anisotropic material that has only diagonal tensor components. The non-axial anisotropic media with non-diagonal tensor components will be studied in Section 3. The permittivity values are considered to have real positive and nonzero values. In this case, the permittivity tensor will be as follows

$$\varepsilon = \begin{bmatrix} \varepsilon_{xx} & 0 \\ 0 & \varepsilon_{yy} \end{bmatrix} = \varepsilon_0 \begin{bmatrix} \varepsilon_{xx}^r & 0 \\ 0 & \varepsilon_{yy}^r \end{bmatrix}. \tag{2}$$

The magnetic permeability of the medium is assumed to be the scalar μ throughout the paper. The anisotropic nature of the domain does not affect the TM mode since in that case, the electric field component is perpendicular to the plane of the electric anisotropy (*xy* plane). Therefore, a TM mode is not influenced by the anisotropy of the electric-anisotropic medium characterized by (2). In this paper, only the TE mode is studied. The dual problem of a TM mode in a magnetic anisotropic medium can be treated in a similar manner. The problem can be generalized to three-dimensional spaces in a straightforward manner.

The anisotropic materials are assumed to be non-dispersive. If the frequency band of interest is far enough from the resonance frequencies, the permittivity, and permeability exhibit a nearly flat behavior and hence they can be approximated by constant values. Therefore the results presented in this paper are valid for flat or nearly flat permittivities and permeabilities. However, the proposed theory is able to be generalized to dispersive media which is a topic of our future research.

The TE Maxwell equations in inhomogeneous axial anisotropic media are as follows

$$\frac{\partial E_x}{\partial t} = \kappa_{xx}(x,y)\frac{\partial H_z}{\partial y}, \tag{3a}$$

$$\frac{\partial E_y}{\partial t} = -\kappa_{yy}(x,y)\frac{\partial H_z}{\partial x}, \tag{3b}$$

$$\frac{\partial H_z}{\partial t} = \frac{1}{\mu}\left(\frac{\partial E_x}{\partial y} - \frac{\partial E_y}{\partial x}\right), \tag{3c}$$

where $\kappa_{xx} = 1/\varepsilon_{xx}$ and $\kappa_{yy} = 1/\varepsilon_{yy}$ are the components of the impermittivity tensor.

Taking the time derivative of (3c) and substituting (3a) and (3b) into the resulting equation yields the second-order wave equation for H_z in the inhomogeneous anisotropic medium as

$$\frac{\partial^2 H_z}{\partial t^2} = \frac{1}{\mu}\left[\left(\frac{\partial \kappa_{xx}}{\partial y}\frac{\partial H_z}{\partial y} + \kappa_{xx}\frac{\partial^2 H_z}{\partial y^2}\right) + \left(\frac{\partial \kappa_{yy}}{\partial x}\frac{\partial H_z}{\partial x} + \kappa_{yy}\frac{\partial^2 H_z}{\partial x^2}\right)\right], \tag{4}$$

Note that the space derivatives of κ_{xx} and κ_{yy} are taken into account since the media are generally assumed to be inhomogeneous. From (3) and Fig. 1, the sampling indices are $E_x(i,j+1/2)$, $E_y(i+1/2,j)$, $H_z(i,j)$, $\kappa_{xx}(i,j+1/2)$, and $\kappa_{yy}(i+1/2,j)$. Therefore, sampling (4) in the FDTD grid yields

$$\begin{aligned} H_z^{n+1}(i,j) = &-H_z^{n-1}(i,j) + C_0 H_z^n(i,j) + C_x^+ H_z^n(i+1,j) \\ &+ C_x^- H_z^n(i-1,j) + C_y^+ H_z^n(i,j+1) \\ &+ C_y^- H_z^n(i,j-1), \end{aligned} \tag{5}$$

where

$$C_x^+ = \frac{\Delta t^2}{\mu \Delta x^2}\kappa_{yy}(i+1/2,j), \tag{6a}$$

$$C_x^- = \frac{\Delta t^2}{\mu \Delta x^2}\kappa_{yy}(i-1/2,j), \tag{6b}$$

$$C_y^+ = \frac{\Delta t^2}{\mu \Delta y^2}\kappa_{xx}(i,j+1/2), \tag{6c}$$

$$C_y^- = \frac{\Delta t^2}{\mu \Delta y^2}\kappa_{xx}(i,j-1/2), \tag{6d}$$

$$C_0 = 2 - \left(C_x^+ + C_x^- + C_y^+ + C_y^-\right), \tag{6e}$$

Following [22], (5) is rewritten as

$$\begin{bmatrix} \mathbf{H}_z^{n+1} \\ \mathbf{H}_z^n \end{bmatrix} = \mathbf{B}\begin{bmatrix} \mathbf{H}_z^n \\ \mathbf{H}_z^{n-1} \end{bmatrix} = \begin{bmatrix} \mathbf{A} & -\mathbf{I} \\ \mathbf{I} & \mathbf{O} \end{bmatrix}\begin{bmatrix} \mathbf{H}_z^n \\ \mathbf{H}_z^{n-1} \end{bmatrix} \tag{7}$$

where $\mathbf{H}_z$ is a vector containing all the samples of H_z in the computational domain, and **I** and **O** are the identity and zero matrices, respectively.

From (7), in a stable algorithm all eigenvalues of the iteration matrix **B** must lie within the unit circle, i.e. $|\lambda_B| \le 1$. Using simple algebraic manipulations, it can be shown that this is identical to $|\lambda_A| \le 2$ [22]. By the use of the Gershgorin circle theorem, one can estimate the permitted regions for the eigenvalues of a matrix in the

complex plane. According to this theorem, the eigenvalues of a matrix lie within circles whose centers are the diagonal entries of the matrix, and whose radii are the sum of the absolute values of the non-diagonal entries of the corresponding row [29]. In other words

$$\left|\lambda_i - a_{ii}\right| \le \sum_{j\neq i}\left|a_{ij}\right|, \tag{8}$$

As a proof of concept, in the following, we consider three basic examples: a homogeneous anisotropic medium, two homogeneous anisotropic media with a flat interface, and an inhomogeneous anisotropic medium.

2.1 A Homogeneous Anisotropic Medium

Fig. 1 illustrates a homogeneous anisotropic medium with nine H_z nodes. The anisotropic medium is represented by κ_{xx} and κ_{yy}. The impermittivities are zero in the PEC region. From (5), (6), and (7), the matrix **A** for this configuration can be derived. If the nine H_z nodes are numbered from left to right, and from bottom to top, the matrix $\mathbf{A}_{9\times 9}$ is obtained as

$$\mathbf{A}=\begin{bmatrix} C_1 & C_x^+ & 0 & C_y^+ & 0 & 0 & 0 & 0 & 0\\ C_x^- & C_2 & C_x^+ & 0 & C_y^+ & 0 & 0 & 0 & 0\\ 0 & C_x^- & C_3 & 0 & 0 & C_y^+ & 0 & 0 & 0\\ C_y^- & 0 & 0 & C_4 & C_x^+ & 0 & C_y^+ & 0 & 0\\ 0 & C_y^- & 0 & C_x^- & C_5 & C_x^+ & 0 & C_y^+ & 0\\ 0 & 0 & C_y^- & 0 & C_x^- & C_6 & 0 & 0 & C_y^+\\ 0 & 0 & 0 & C_y^- & 0 & 0 & C_7 & C_x^+ & 0\\ 0 & 0 & 0 & 0 & C_y^- & 0 & C_x^- & C_8 & C_x^+\\ 0 & 0 & 0 & 0 & 0 & C_y^- & 0 & C_x^- & C_9 \end{bmatrix}, \tag{9}$$

where the diagonal entries are the sum of the non-diagonal entries of their corresponding row subtracted from 2.

The fifth row pertains to the central node in Fig. 1. Applying the Gershgorin theorem to this row and upon using (6), one obtains

$$\left|\lambda - 2 + \frac{2\Delta t^2}{\mu}\left(\frac{\kappa_{xx}}{\Delta y^2}+\frac{\kappa_{yy}}{\Delta x^2}\right)\right| \le \frac{2\Delta t^2}{\mu}\left(\frac{\kappa_{xx}}{\Delta y^2}+\frac{\kappa_{yy}}{\Delta x^2}\right), \tag{10}$$

It can be shown that all the eigenvalues of **A** are real values [29]. On the other hand, to ensure stability, the eigenvalues of **A** must lie within a circle of radius 2, i.e. $|\lambda_A| \le 2$. Hence from (10), the CFL condition for the anisotropic medium is obtained as

$$\Delta t \le \frac{\sqrt{\mu}}{\sqrt{\frac{\kappa_{yy}}{\Delta x^2}+\frac{\kappa_{xx}}{\Delta y^2}}} = \Delta t_{CFL}, \tag{11}$$

Since the CFL time step in (11) corresponds to the central node, whose adjacent E_x and E_y nodes are all in the same medium, it represents the CFL condition in an unbounded homogeneous anisotropic medium. Assuming $\kappa_{xx} = \kappa_{yy} = 1/\varepsilon$, (11) reduces to (1), which is the CFL condition in isotropic media. Other rows of the matrix pertain to the H_z nodes adjacent to the PEC boundaries, i.e. boundary nodes. Applying the Gershgorin theorem to those rows yields upper bounds for Δt which are not as restrictive as (11). This is due to the fact that some terms in the denominator of the time step will vanish and the resulting CFL condition will be larger than (11). Particularly, the edge nodes yield more relaxed CFL conditions than other boundary nodes. Therefore the CFL constraint given by (11) is the determinative CFL condition across the entire domain.

It is important to note that the Gershgorin theorem guarantees that the time step (11) falls inside the permitted values of the time steps. In other words, (11) gives a sufficient condition for stability. However, the actual permitted time step of the time marching algorithm $\Delta t_{\max}$ may be slightly larger than (11). As we will observe in the results section, $\Delta t_{\max}$ converges to Δt_{CFL} as the grid size increases. This is in agreement with the results obtained for the finite isotropic media [21, 23]. In the proposed method it is not possible to study analytically the effect of grid size on the maximum permitted time step and hence this task is performed numerically.

2.2 Two Homogeneous Anisotropic Media with a Flat Interface

Fig. 2 illustrates two homogeneous anisotropic media with a flat interface. The left and right media are represented by the permittivity tensors $\boldsymbol{\varepsilon}_1$ and $\boldsymbol{\varepsilon}_2$, respectively. Assume a uniform mesh across the entire domain.

From (11), the CFL time steps for the left and right media are

$$\Delta t_{CFL1} = \frac{\sqrt{\mu}}{\sqrt{\frac{\kappa_{yy1}}{\Delta x^2}+\frac{\kappa_{xx1}}{\Delta y^2}}}, \quad \Delta t_{CFL2} = \frac{\sqrt{\mu}}{\sqrt{\frac{\kappa_{yy2}}{\Delta x^2}+\frac{\kappa_{xx2}}{\Delta y^2}}}, \tag{12}$$

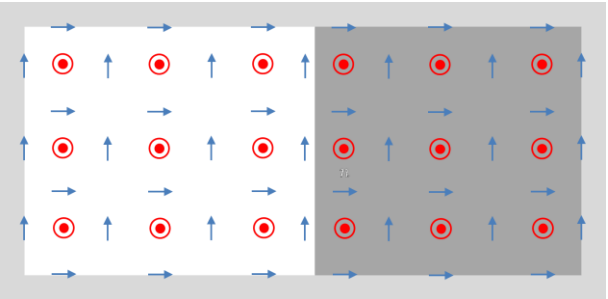

Fig. 2 The TE computational space enclosed by a PEC boundary and filled with two homogeneous anisotropic media.

Here we are interested in the CFL condition imposed by the interface. Deriving the matrix $\mathbf{A}_{18\times18}$ from (6) and (7), and applying the Gershgorin theorem to the row pertaining to the node n, which is the H_z node adjacent to the interface, one obtains the following CFL condition

$$\Delta t_{CFL\,\mathrm{int}} = \frac{\sqrt{\mu}}{\sqrt{\dfrac{\left(\kappa_{yy1}+\kappa_{yy2}\right)/2}{\Delta x^2}+\dfrac{\kappa_{xx2}}{\Delta y^2}}}, \tag{13}$$

The CFL condition pertaining to the node n' is equal to Δt_{CFL1}, since the four electric field nodes surrounding n' are all located inside medium 1.

The CFL time steps in (12) are the bounds imposed by the two media regardless of the interface, while (13) is the bound imposed by the interface. The most restrictive one is equal to the minimum of the three time steps. Note that applying the Gershgorin theorem to the nodes adjacent to the PEC boundaries yields more relaxed conditions and hence they are not determinative.

If $\kappa_{xx1} \le \kappa_{xx2}$ and $\kappa_{yy1} \le \kappa_{yy2}$, or $\kappa_{xx1} \ge \kappa_{xx2}$ and $\kappa_{yy1} \ge \kappa_{yy2}$, it is easy to show that

$$\Delta t_{\mathrm{CFL\,int}} \ge \min\left(\Delta t_{\mathrm{CFL1}}, \Delta t_{\mathrm{CFL2}}\right), \tag{14}$$

Therefore, in this case, the CFL time step imposed by the interface is not determinative. If $\kappa_{xx1} \ge \kappa_{xx2}$ and $\kappa_{yy1} \ge \kappa_{yy2}$, the medium 1 offers the most restrictive CFL condition. Conversely if $\kappa_{xx1} \le \kappa_{xx2}$ and $\kappa_{yy1} \le \kappa_{yy2}$, the medium 2 offers the most restrictive CFL time step. If $\kappa_{xx1} \ge \kappa_{xx2}$ and $\kappa_{yy1} \le \kappa_{yy2}$, the smallest time step is among Δt_{CFL1} and Δt_{CFL2}. It is easy to show that Δt_{CFL2} is the most restrictive time step when

$$\frac{\Delta y}{\Delta x} \ge \sqrt{\frac{\kappa_{xx1}-\kappa_{xx2}}{\kappa_{yy2}-\kappa_{yy1}}}, \tag{15}$$

where $\Delta y/\Delta x$ is the unit cell aspect ratio. If (15) is not satisfied, Δt_{CFL1} will be the most restrictive time step. If $\kappa_{xx1} \le \kappa_{xx2}$ and $\kappa_{yy1} \ge \kappa_{yy2}$, the smallest time step is among Δt_{CFL1} and $\Delta t_{\mathrm{CFLint}}$. For the following inequality

$$\frac{\Delta y}{\Delta x} \ge \sqrt{2}\sqrt{\frac{\kappa_{xx2}-\kappa_{xx1}}{\kappa_{yy1}-\kappa_{yy2}}} \tag{16}$$

the time step Δt_{CFL1} is the most restrictive one. Otherwise, $\Delta t_{\mathrm{CFLint}}$ will be the determinative CFL time step across the entire space. This is an important result and shows that in this case the von-Neumann criterion, which does not take the effect of the interface into account, is not able to predict the stability bound. Table 1 summarizes the results.

It is useful to study the stability behavior of isotropic media at their interface as a special case of anisotropic media. It is obvious that when $\kappa_{xx1} = \kappa_{yy1} = \kappa_1$ and $\kappa_{xx2} = \kappa_{yy2} = \kappa_2$, (12) reduces to the well-known CFL relation in isotropic media. As stated above, in anisotropic media four relations can be defined between the four quantities κ_{xx1}, κ_{xx2}, κ_{yy1}, and κ_{yy2}, which are expressed in Table 1, column 1. For isotropic media there are only two relations: $\kappa_1 \ge \kappa_2$ and $\kappa_1 \le \kappa_2$, which from (12) and (13), denote that the most restrictive CFL condition pertains to the medium 1 and medium 2, respectively. In the presence of isotropic media, the conditions expressed in the last four rows of Table 1 are no longer meaningful. In agreement with this fact, the expressions in the second column pertaining to the unit cell aspect ratios become imaginary. Hence the interface between two isotropic media has no restrictive effect on the CFL condition of the grid, and the medium with the largest impermittivity determines the CFL condition across the entire domain.

Table 1 The CFL conditions in axial anisotropic media depicted in Fig. 2 for different impermittivities and unit cell aspect ratios.

Condition 1	Condition 2	The CFL Time Step
$\kappa_{xx1} \le \kappa_{xx2}$ $\kappa_{yy1} \le \kappa_{yy2}$	----------	Δt_{CFL2}
$\kappa_{xx1} \ge \kappa_{xx2}$ $\kappa_{yy1} \ge \kappa_{yy2}$	----------	Δt_{CFL1}
$\kappa_{xx1} \ge \kappa_{xx2}$ $\kappa_{yy1} \le \kappa_{yy2}$	$\dfrac{\Delta y}{\Delta x} \ge \sqrt{\dfrac{\kappa_{xx1}-\kappa_{xx2}}{\kappa_{yy2}-\kappa_{yy1}}}$	Δt_{CFL2}
$\kappa_{xx1} \ge \kappa_{xx2}$ $\kappa_{yy1} \le \kappa_{yy2}$	$\dfrac{\Delta y}{\Delta x} \le \sqrt{\dfrac{\kappa_{xx1}-\kappa_{xx2}}{\kappa_{yy2}-\kappa_{yy1}}}$	Δt_{CFL1}
$\kappa_{xx1} \le \kappa_{xx2}$ $\kappa_{yy1} \ge \kappa_{yy2}$	$\dfrac{\Delta y}{\Delta x} \ge \sqrt{2}\sqrt{\dfrac{\kappa_{xx2}-\kappa_{xx1}}{\kappa_{yy1}-\kappa_{yy2}}}$	Δt_{CFL1}
$\kappa_{xx1} \le \kappa_{xx2}$ $\kappa_{yy1} \ge \kappa_{yy2}$	$\dfrac{\Delta y}{\Delta x} \le \sqrt{2}\sqrt{\dfrac{\kappa_{xx2}-\kappa_{xx1}}{\kappa_{yy1}-\kappa_{yy2}}}$	$\Delta t_{\mathrm{CFLint}}$

2.3 An Inhomogeneous Medium

In this part, we generalize the problem and consider an inhomogeneous anisotropic medium with a permittivity tensor gradually varying with the position. When modeling this medium in the FDTD algorithm, the gradual variation in the permittivity will be discretized into permittivity jumps in the grid. Fig. 3 shows a small portion of this medium in the computational grid. Each color denotes a different amount of permittivity tensor. A special category among inhomogeneous media that usually encounters in practical applications is a heterogeneous medium, i.e. a finite number of homogeneous objects.

If the inhomogeneous medium depicted in Fig. 3 is isotropic, from the results discussed above one concludes that the unit cell (pixel) with the largest impermittivity κ (the smallest permittivity ε) imposes the most restrictive CFL condition on the whole grid.

$$\Delta t_{\mathrm{CFL}}(i,j)=\frac{\sqrt{2\mu}}{\sqrt{\dfrac{\kappa_{yy}(i+1/2,j)+\kappa_{yy}(i-1/2,j)}{\Delta x(i,j)^2}+\dfrac{\kappa_{xx}(i,j+1/2)+\kappa_{xx}(i,j-1/2)}{\Delta y(i,j)^2}}} \tag{17}$$

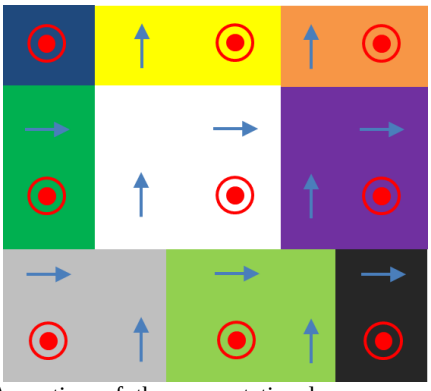

Fig. 3 A portion of the computational space sampling an inhomogeneous anisotropic medium.

Now we turn back to the problem of anisotropic media. To make the problem more general, a non-uniform gridding scheme is assumed. In this case, Δx and Δy are functions of the position. Then, applying the Gershgorin theorem to a generic H_z node located at (i,j), CFL condition (17) is obtained, which generally varies over the grid nodes. The impermittivities located inside the PEC boundaries are set to zero. To determine the most restrictive CFL condition it is enough to find the minimum value of the time steps in (17) over the entire domain, i.e.

$$\Delta t_{\mathrm{CFL}}=\min_{i,j}\left\{\Delta t_{\mathrm{CFL}}(i,j)\right\}, \tag{18}$$

Remind that the actual permitted time step $\Delta t_{\max}$ of the grid may be slightly larger than the CFL time step given by (18). As the grid size increases, $\Delta t_{\max}$ converges to (18). In the literature, $\Delta t_{\max}$ in a bounded computational space is generally determined by a tedious numerical treatment of the eigenvalues of the iteration matrix [19]. For a grid size of $M\times N$, the size of the iteration matrix will be $MN\times MN$ which increases tremendously with the size of the grid. Consequently, for practical applications determining $\Delta t_{\max}$ is very time-consuming. Instead, (17) and (18) rapidly give Δt_{CFL} as a very close approximation of $\Delta t_{\max}$, where for large grid sizes the two time steps will converge. Equation (17) is a point-wise relation and hence can detect the point which imposes the most restrictive CFL condition and may be a potential source of instability. This is particularly useful in studying the stability in flat, tilted, or curved interfaces.

3 Generalization of the Theory to Non-Axial Anisotropic Media

We now assume that the electric permittivity is a non-axial tensor, i.e.

$$\boldsymbol{\varepsilon}=\begin{bmatrix}\varepsilon_{xx} & \varepsilon_{xy}\\ \varepsilon_{yx} & \varepsilon_{yy}\end{bmatrix}=\varepsilon_0\begin{bmatrix}\varepsilon^r_{xx} & \varepsilon^r_{xy}\\ \varepsilon^r_{yx} & \varepsilon^r_{yy}\end{bmatrix}, \tag{19}$$

This tensor arises when the FDTD grid is not aligned with the principal axes of the anisotropic medium. Assuming that the medium is reciprocal, it can be shown that the non-diagonal entries are equal, i.e. $\varepsilon_{xy}=\varepsilon_{yx}$ [2]. However, their location in the staggered FDTD grid is different; and hence different notations are used to represent them. This is important in inhomogeneous and heterogeneous media. In a reciprocal non-axial anisotropic medium the coordinate system can be aligned with the principal axis of the medium and hence the dielectric tensor becomes axial [2]. However, in a computational space, several non-axial anisotropic media with different principal axes may exist. In this case, it is not possible to align the FDTD grid with all principal axes.

In non-axial media the TE Maxwell equations are

$$\frac{\partial E_x}{\partial t}=\kappa_{xx}(x,y)\frac{\partial H_z}{\partial y}-\kappa_{xy}(x,y)\frac{\partial H_z}{\partial x}, \tag{20a}$$

$$\frac{\partial E_y}{\partial t}=\kappa_{yx}(x,y)\frac{\partial H_z}{\partial y}-\kappa_{yy}(x,y)\frac{\partial H_z}{\partial x}, \tag{20b}$$

$$\frac{\partial H_z}{\partial t}=\frac{1}{\mu}\left(\frac{\partial E_x}{\partial y}-\frac{\partial E_y}{\partial x}\right), \tag{20c}$$

where κ_{xy} and κ_{yx} are the non-diagonal components of the impermittivity matrix. Following a similar procedure as in Section 2, the following wave equation is obtained

$$\begin{aligned}\frac{\partial^2 H_z}{\partial t^2}=&\\ &\frac{1}{\mu}\left[\left(\frac{\partial \kappa_{xx}}{\partial y}\frac{\partial H_z}{\partial y}+\kappa_{xx}\frac{\partial^2 H_z}{\partial y^2}\right)-\left(\frac{\partial \kappa_{xy}}{\partial y}\frac{\partial H_z}{\partial x}+\kappa_{xy}\frac{\partial^2 H_z}{\partial x\partial y}\right)\right]\\ &-\frac{1}{\mu}\left[\left(\frac{\partial \kappa_{yx}}{\partial x}\frac{\partial H_z}{\partial y}+\kappa_{yx}\frac{\partial^2 H_z}{\partial x\partial y}\right)-\left(\frac{\partial \kappa_{yy}}{\partial x}\frac{\partial H_z}{\partial x}+\kappa_{yy}\frac{\partial^2 H_z}{\partial x^2}\right)\right],\end{aligned} \tag{21}$$

From (20), and following the gridding scheme in Fig. 1, the locations of the non-diagonal components are $\kappa_{xy}(i,j+1/2)$ and $\kappa_{yx}(i+1/2,j)$. Hence, using the central differencing and performing a spatial interpolation from four neighboring nodes to associate the non-collocated field components, the finite difference form of (21) can be cast in the following form

$$H_z^{n+1}(i,j) = -H_z^{n-1}(i,j) + C_0 H_z^n(i,j) + C_x^+ H_z^n(i+1,j) + C_x^- H_z^n(i-1,j) + C_y^+ H_z^n(i,j+1) + C_y^- H_z^n(i,j-1) - C_1\left[H_z^n(i+1,j+1) - H_z^n(i+1,j-1) - H_z^n(i-1,j+1) + H_z^n(i-1,j-1)\right], \quad (22)$$

where the coefficients are given in Appendix A. Applying the Gershgorin theorem to (22) yields the following CFL bound in a generic inhomogeneous non-axial anisotropic medium

$$\Delta t_{CFL}(i,j) = \frac{2\sqrt{\mu}}{\sqrt{4D_1 + D_x^+ + D_x^- + D_y^+ + D_y^- + \left|D_x^+\right| + \left|D_x^-\right| + \left|D_y^+\right| + \left|D_y^-\right|}}, \quad (23)$$

where D_1, D^+_x, D^-_x, D^+_y, and D^-_y are shown in Appendix A. In (23) the unit cell dimensions can be functions of the position. The most restrictive CFL time step is equal to the minimum of (23) over the entire space. In a PEC boundary, the values of impermittivities are set to zero.

For a special case of a homogeneous medium, (23) reduces to

$$\Delta t_{CFL} = \frac{2\sqrt{\mu}}{\sqrt{4\left(\frac{\kappa_{yy}}{\Delta x^2} + \frac{\kappa_{xx}}{\Delta y^2}\right) + \frac{\kappa_{xy} + \kappa_{yx}}{\Delta x \Delta y}}}, \quad (24)$$

From (24) it is clear that due to the presence of nonzero cross components (κ_{xy} and κ_{yx}) the CFL time step in a non-axial anisotropic medium is smaller than that of an axial anisotropic medium given by (11). For a reciprocal homogeneous medium, in which $\kappa_{xy} = \kappa_{yx}$, (24) reduces to

$$\Delta t_{CFL} = \frac{\sqrt{2\mu}}{\sqrt{2\left(\frac{\kappa_{yy}}{\Delta x^2} + \frac{\kappa_{xx}}{\Delta y^2}\right) + \frac{\kappa_{xy}}{\Delta x \Delta y}}}, \quad (25)$$

Assume that the materials in Fig. 2 are two non-axial reciprocal media. Applying (23) to the node *n*, adjacent to the interface, the CFL time step at the interface is determined which is a piecewise function due to the existence of absolute values in the denominator of (23). For $\kappa_{xy1} = \kappa_{xy2} = \kappa_{xy}$ it is

$$\Delta t_{CFLint} = \frac{2\sqrt{\mu}}{\sqrt{\frac{2\left(\kappa_{yy1} + \kappa_{yy2}\right)}{\Delta x^2} + \frac{4\kappa_{xx2}}{\Delta y^2} + \frac{2\kappa_{xy}}{\Delta x \Delta y}}}, \quad (26)$$

For $\kappa_{xy1} \neq \kappa_{xy2}$ and $\Delta y/\Delta x \leq 2\kappa_{xx2}/|\kappa_{xy2} - \kappa_{xy1}|$ it is equal to

$$\Delta t_{CFLint} = \frac{2\sqrt{\mu}}{\sqrt{\frac{2\left(\kappa_{yy1} + \kappa_{yy2}\right)}{\Delta x^2} + \frac{4\kappa_{xx2}}{\Delta y^2} + \frac{\kappa_{xy1} + 3\kappa_{xy2}}{2\Delta x \Delta y}}}, \quad (27)$$

For $\kappa_{xy1} < \kappa_{xy2}$ and $\Delta y/\Delta x \geq 2\kappa_{xx2}/(\kappa_{xy2} - \kappa_{xy1})$ it becomes

$$\Delta t_{CFLint} = \frac{2\sqrt{\mu}}{\sqrt{\frac{2\left(\kappa_{yy1} + \kappa_{yy2}\right)}{\Delta x^2} + \frac{2\kappa_{xx2}}{\Delta y^2} + \frac{-\kappa_{xy1} + 5\kappa_{xy2}}{2\Delta x \Delta y}}}, \quad (28)$$

Finally, for $\kappa_{xy1} > \kappa_{xy2}$ and $\Delta y/\Delta x \geq 2\kappa_{xx2}/(\kappa_{xy1} - \kappa_{xy2})$ it equals to

$$\Delta t_{CFLint} = \frac{2\sqrt{\mu}}{\sqrt{\frac{2\left(\kappa_{yy1} + \kappa_{yy2}\right)}{\Delta x^2} + \frac{2\kappa_{xx2}}{\Delta y^2} + \frac{3\kappa_{xy1} + \kappa_{xy2}}{2\Delta x \Delta y}}}, \quad (29)$$

Following the procedure in Section 2.2, one can compare the values of Δt_{CFLint}, Δt_{CFL1}, and Δt_{CFL2} and derive the closed-form relations for the pertaining conditions. However, several conditions and formulations arise which are not reported here for brevity.

4 Results and Discussion

In this section, some examples of electromagnetic wave propagation in anisotropic media are studied as proofs of concept. In the verifications, homogeneous and inhomogeneous media and also axial and non-axial permittivity tensors are considered.

4.1 A Homogeneous Axial Anisotropic Medium

The configuration under study is similar to Fig. 1 with a 10×10 grid size. Assume that $\varepsilon^r_{xx} = 2$, and $\varepsilon^r_{yy} = 3$ are the relative permittivities of the medium, and $dy = dx = 2$ μm are the cell sizes. After derivation of **A**, the eigenvalues of the iteration matrix **B** are calculated. Fig. 4 depicts the eigenvalues of **B** for several values of the time step. The eigenvalues are complex conjugate and hence it is enough to depict them in the upper semicircles. From Fig. 4(a) when the time step is smaller than or equal to the CFL limit, the eigenvalues of the iteration matrix are located on the unit circle. For very small time steps, the eigenvalues shrink to a region on the circle which is close to 1. As the time step increases, they distribute around the circle. As it is observed from Fig. 4(b), for the time steps larger than the CFL limit real eigenvalues emerge; half of which are inside the circle and other half are outside the circle resulting in instability. The absolute values of the real eigenvalues outside the unit circle increase with the time step, and hence the instability occurs earlier.

In small size grids, the maximum allowable time step Δt_{max} obtained from the eigenvalue analysis is slightly larger than the CFL limit Δt_{CFL} given by (11). However, as the grid size increases Δt_{max} rapidly converges to (11). Table 2 shows the ratio $\Delta t_{max}/\Delta t_{CFL}$ for the configuration given in Fig. 1. It is assumed that the numbers of the cells in both directions are equal, i.e. $M = N$. For $M \geq 12$, Δt_{max} reduces to Δt_{CFL}. It is evident that

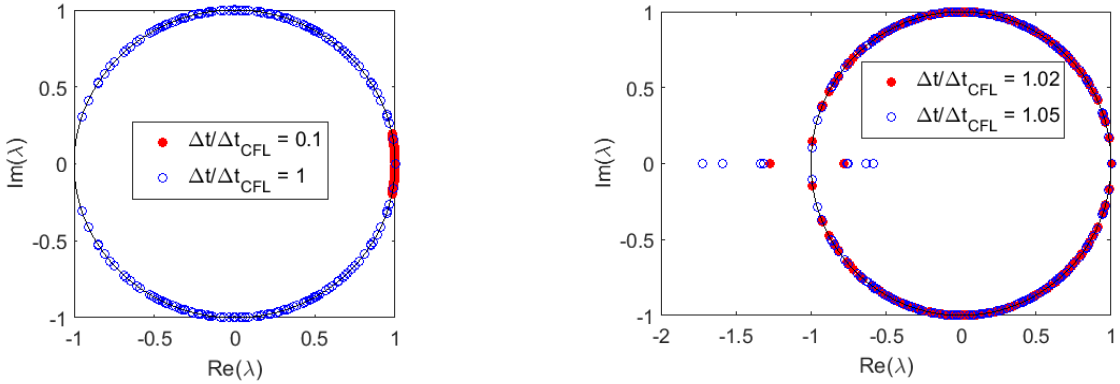

Fig. 4 The eigenvalues of **B** in a homogeneous anisotropic medium for a) $\Delta t/\Delta t_{CFL} = 0.1$, and $\Delta t/\Delta t_{CFL} = 1$ and b) $\Delta t/\Delta t_{CFL} = 1.02$ and $\Delta t/\Delta t_{CFL} = 1.05$.

Table 2 The Ratio $\Delta t_{max}/\Delta t_{CFL}$ as a function of the grid size.

M	$\Delta t_{max}/\Delta t_{CFL}$	M	$\Delta t_{max}/\Delta t_{CFL}$
5	1.05	11	1.01
6	1.03	12	1.00
7	1.02	13	1.00
8	1.01	14	1.00
9	1.01	15	1.00
10	1.01	16	1.00

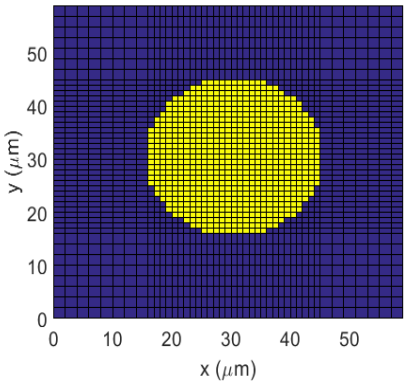

Fig. 5 An anisotropic cylinder embedded in free space. An adaptive gridding scheme is used.

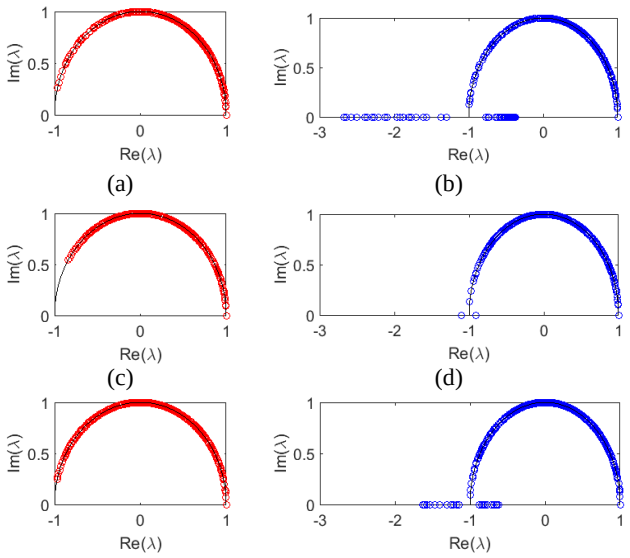

Fig. 6 The eigenvalues of **B** in a space including two axial anisotropic homogeneous media with a flat interface; a) $\Delta t = \Delta t_{CFL2}$, b) $\Delta t = \Delta t_{CFLint}$, (In (a) and (b): $\varepsilon^r_{xx1} = 4$, $\varepsilon^r_{yy1} = 3$, $\varepsilon^r_{xx2} = 2$, $\varepsilon^r_{yy2} = 1$, and $dy = dx$), c) $\Delta t = \Delta t_{CFLint}$, d) $\Delta t = \Delta t_{CFL1}$, (In (c) and (d): $\varepsilon^r_{xx1} = 2$, $\varepsilon^r_{yy1} = 3$, $\varepsilon^r_{xx2} = 1$, $\varepsilon^r_{yy2} = 6$, and $dy = 2dx$), e) $\Delta t = \Delta t_{CFL1}$, and f) $\Delta t = \Delta t_{CFLint}$, (In (e) and (f): $\varepsilon^r_{xx1} = 2$, $\varepsilon^r_{yy1} = 3$, $\varepsilon^r_{xx2} = 1$, $\varepsilon^r_{yy2} = 6$, and $dy = 3dx$).

in practical applications, the grid size is usually much larger than those given in Table 2.

5.2 Two Homogeneous Axial Anisotropic Media with a Flat Interface

Assume that the space shown in Fig. 2 is sampled with a 20×20 grid. The media have axial anisotropic tensors. Half of the nodes are inside medium 1, and the other half is inside medium 2. To verify the results shown in Table 1, the simulations are performed for various values of the impermittivities and unit cell aspect ratios, and the eigenvalues are depicted in Fig. 5. For each case, the eigenvalues of the iteration matrix **B** are computed for the two smallest CFL limits among the three limits given in (12) and (13). As it is observed, the results follow the predictions of Table 1. In Fig. 5(d) the time step is equal to the smaller CFL time step among Δt_{CFL1} and Δt_{CFL2}. However, the algorithm is unstable since the aspect ratio of the unit cells is selected such that the determinative factor is the CFL limit imposed by the interface. In this case, it is evident that the von-Neumann criterion cannot predict the minimum CFL time step over the computational space.

5.3 An Axial Anisotropic Cylinder

Fig. 6 depicts a homogeneous axial anisotropic

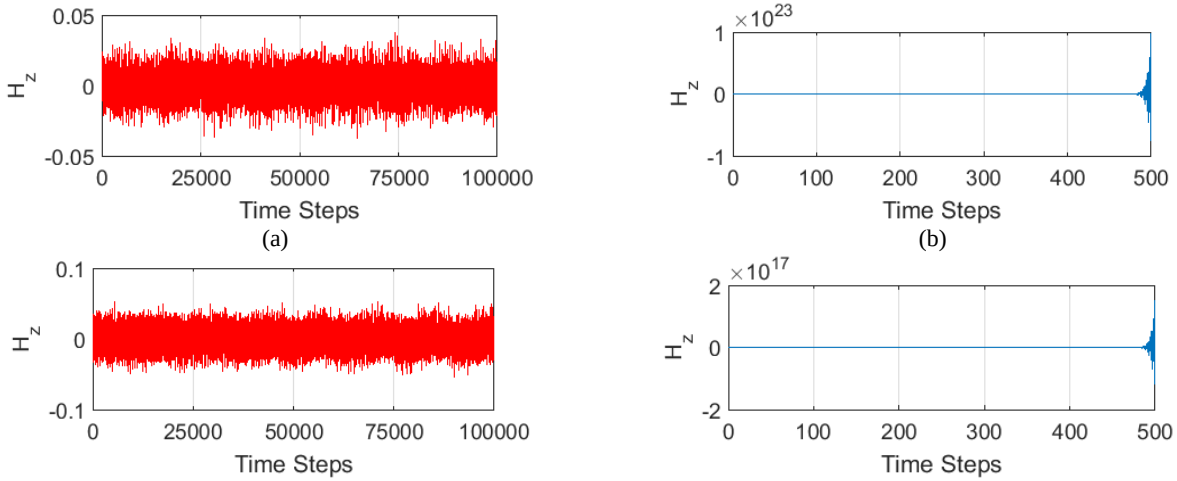

Fig. 7 The magnetic field H_z as a function of time in the presence of an axial anisotropic cylinder; a) $\Delta t = \Delta t_{CFL}$, b) $\Delta t = 1.01\Delta t_{CFL}$, ((a) and (b) pertain to the homogeneous cylinder), c) $\Delta t = \Delta t_{CFL}$, and d) $\Delta t = 1.01\Delta t_{CFL}$, ((c) and (d) pertain to the inhomogeneous cylinder).

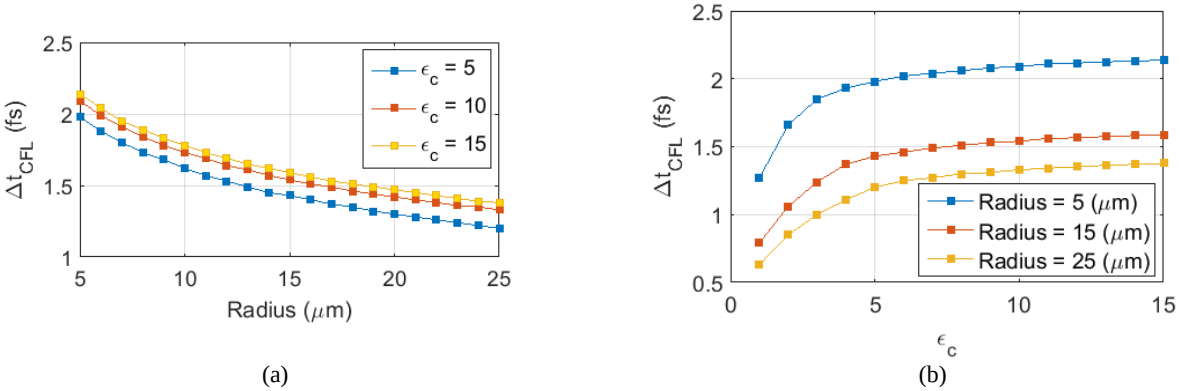

Fig. 8 a) Δt_{CFL} as a function of the cylinder radius for different values of $\boldsymbol{\varepsilon}_c$ and b) Δt_{CFL} as a function of $\boldsymbol{\varepsilon}_c$ for different values of the cylinder radius.

cylinder of radius $15\mu m$ with $\varepsilon^r_{xx} = 8$, and $\varepsilon^r_{yy} = 12$, which is embedded in free space. The cylinder is located at the center of a 60μm×60μm computational space. An adaptive gridding scheme is used to refine the details in modeling the cylinder. In the cylindrical region $dx = dy$ = 1 μm, and in the surrounding space three types of unit cells are used to model various regions: $dx = dy$ = 2μm, $2dx = dy$ = 2 μm, and $dx = 2dy$ = 2 μm. These regions can be distinguished in Fig. 6. A staircase approximation is utilized to model the curved boundaries.

From (17) and (18), the CFL time step is computed as Δt_{CFL} = 2.36 Femtoseconds, which pertains to the region inside the free space with the smallest unit cells. The space is excited at (x,y) = (50 μm,50 μm) by the Gaussian pulse $\exp[-(t-t_0)^2/\tau]$, where $\tau = 3.6t_0$. Fig. 7(a) and Fig. 7(b) depict the magnetic field H_z at (x,y) = (20 μm,20 μm). For $\Delta t = \Delta t_{CFL}$, the field is computed for 100000 time steps which clearly remains stable. However, for $\Delta t = 1.01\Delta t_{CFL}$ the instability emerges after a few hundred time steps.

Now we assume that the cylinder depicted in Fig. 6 is an inhomogeneous axial anisotropic cylinder with the permittivity components defined by

$$\varepsilon^r_{xx} = \varepsilon_c \frac{1+\cos^2\varphi}{r+2}, \quad \varepsilon^r_{yy} = \frac{1+\sin^2\varphi}{\sqrt{r+1}}, \tag{30}$$

where r (in μm) and φ are the radius and angle in polar coordinates, and ε_c = 10 is a parameter. In this case, from (17) and (18) the CFL time step is computed as Δt_{CFL} = 1.54 Femtoseconds. Fig. 7(c) and Fig. 7(d) show H_z at (x,y) = (20μm,20μm) computed for $\Delta t = \Delta t_{CFL}$ and $\Delta t = 1.01\Delta t_{CFL}$. The waveform is stable for the former time step and it is unstable for the latter one.

By using the closed-form relation (17), the parametric analysis of the bounds on the time steps becomes straightforward and rapid. Fig. 8(a) illustrates the CFL time step Δt_{CFL} as a function of the radius of the inhomogeneous cylinder for different values of ε_c. The value of Δt_{CFL} decreases with the radius and increases with ε_c. Fig. 8(b) shows Δt_{CFL} as a function of ε_c for

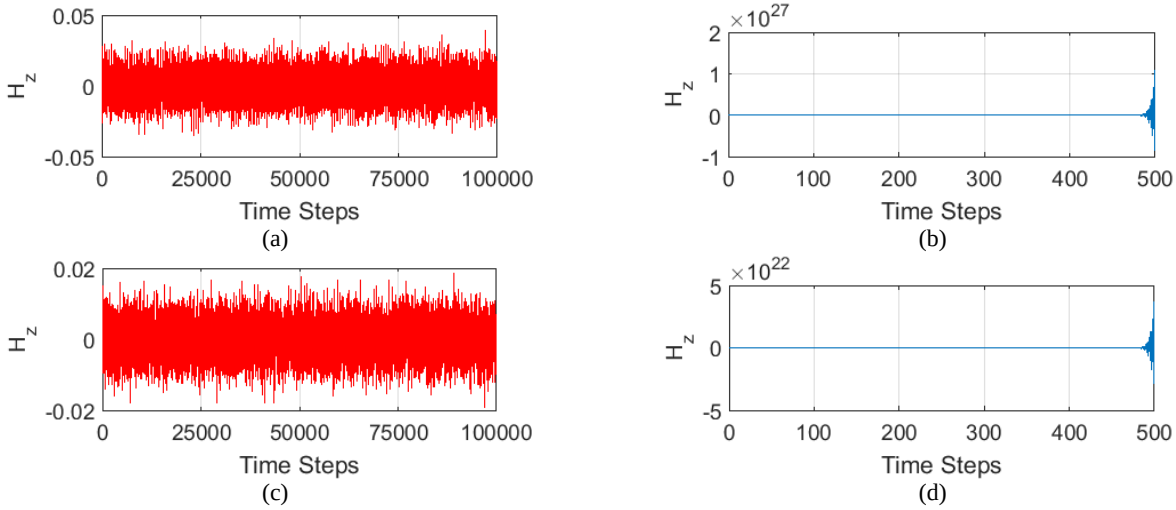

Fig. 9 The magnetic field H_z as a function of time in a non-axial anisotropic medium; a) $\Delta t = \Delta t_{CFL}$, b) $\Delta t = 1.01\Delta t_{CFL}$, ((a) and (b) pertain to the homogeneous medium), c) $\Delta t = \Delta t_{CFL}$, and d) $\Delta t = 1.01\Delta t_{CFL}$, ((c) and (d) pertain to the inhomogeneous medium).

different values of the radius. For large values of ε_c, Δt_{CFL} approaches constant values.

5.4 Non-Axial Anisotropic Media

With reference to Fig. 1, assume a PEC-enclosed homogeneous reciprocal non-axial anisotropic medium with the relative impermittivity components κ^r_{xx} =1/ 5, $\kappa^r_{xy} = \kappa^r_{yx}$ = 1/3, and κ^r_{yy} = 1/4. The computational space is sampled with 21×21 H_z nodes. The unit cell dimensions are assumed to be $dx = dy$ = 1 μm. From (25) the CFL time step is calculated as Δt_{CFL} = 4.25 Femtoseconds. The point (x,y) = (5 μm,10 μm) is excited with a Gaussian pulse $\exp[-(t\text{-}t_0)^2/\tau]$, where $\tau = 3.6t_0$. Fig. 9(a) and Fig. 9(b) depict the magnetic field H_z at (x,y) = (10 μm,5 μm). For $\Delta t = \Delta t_{CFL}$, the field is computed for 100000 time steps which clearly remains stable. However, for $\Delta t = 1.01\Delta t_{CFL}$ the instability emerges after a few hundred time steps.

Now we consider the configuration in Fig. 6 where the cylinder is an inhomogeneous non-axial anisotropic medium with the following permittivity profile

$$\varepsilon^r_{xx} = |x|/3+1,\ \varepsilon^r_{yy} = |y|+0.5,\quad \varepsilon^r_{xy} = \varepsilon^r_{yx} = \sqrt{|xy|/20+1}, \quad (31)$$

where x and y are in μm and the point (x = 0, y = 0) corresponds to the central H_z node. The excitation and observation points are the same as in Section 4.3. The impermittivity components at the cylindrical boundary are modified based on Yu-Mittra subcell modeling [30]. Fig. 10 shows a portion of the boundary. In this case, the effective impermittivities at the boundary are

$$\kappa_{xx/xy,eff}\left(i, j-1/2\right) = \frac{\left(\Delta x-\delta x\right)\kappa_{xx/xy}+\delta x\kappa_0}{\Delta x}, \quad (32a)$$

$$\kappa_{yx/yy,\text{eff}}\left(i-1/2, j\right) = \frac{\left(\Delta y-\delta y\right)\kappa_{yx/yy}+\delta y\kappa_0}{\Delta y}, \quad (32b)$$

where $\kappa_0 = 1/\varepsilon_0$, and κ_{xx}, κ_{xy}, κ_{yx}, and κ_{yy} pertain to the cylinder material. The notation $\kappa_{xx/xy}$ means that (32a) holds for both components κ_{xx} and κ_{xy}. The same expression holds for $\kappa_{yx/yy}$ in (32b). The impermittivities in (32) are substituted in the CFL condition (23), where it yields the CFL time step Δt_{CFL} = 1.78 Femtoseconds. Fig. 9(c) and Fig. 9(d) depict the magnetic field H_z. As it is evident, the time domain simulations verify the proposed theory.

5.5 Two Homogeneous Non-Axial Anisotropic Media with a Flat Interface

Assume that the space depicted in Fig. 2 is sampled with a 30×30 grid. The media have non-axial anisotropic permittivity tensors. Half of the nodes are inside medium 1, and the other half is inside medium 2. Assume that $3dx = dy$ = 3 μm, (κ^r_{xx1} = 1/2, κ^r_{xy1} = 10/3, κ^r_{yy1} = 1/3) and (κ^r_{xx2} = 1, κ^r_{xy2} = 10, κ^r_{yy2} = 1/6), then from (25) and (28) the CFL time steps are calculated as Δt_{CFL1} = 3.43, Δt_{CFL2} = 2.39, and Δt_{CFLint} = 2.22 Femtoseconds. In this case, the stability is constrained by the interface CFL condition. Fig. 11 shows the eigenvalues of the computational space calculated for $\Delta t = \Delta t_{CFL2}$. Although the time step falls within the permitted range offered by the von-Neumann condition, instability arises in the grid.

6 Conclusion

In this paper, we proposed a simple and accurate method to derive the stability bounds of the FDTD algorithm in a generic inhomogeneous or heterogeneous anisotropic medium. The permittivity tensors can be either axial or non-axial. The theory is based on the Gershgorin circle theorem applied to the wave equation in which the permitted regions for the eigenvalues of the iteration matrix in the complex plane are determined.

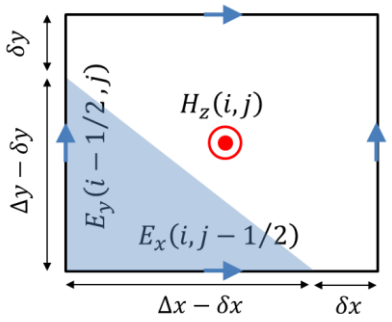

Fig. 10 A portion of the boundary between the non-axial anisotropic cylinder and free space modeled by Yu-Mittra formalism.

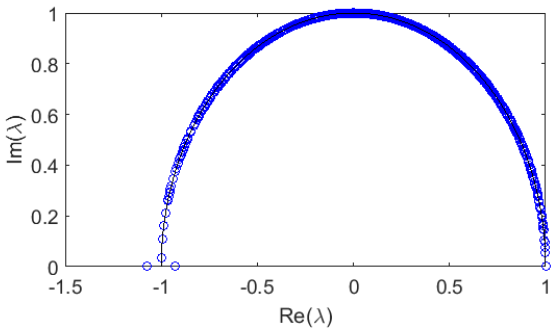

Fig. 11 The eigenvalues of B in a space including two non-axial anisotropic homogeneous media with a flat interface for $\varepsilon^r_{xx1} = 2$, $\varepsilon^r_{xy1} = 0.3$, $\varepsilon^r_{yy1} = 3$, and $\varepsilon^r_{xx2} = 1$, $\varepsilon^r_{xy2} = 0.1$, $\varepsilon^r_{yy2} = 6$. Assume that $3dx = dy = 3$ μm and $\Delta t = \Delta t_{CFL2}$.

Then the sufficient stability conditions imposed on the time step are derived. The formulations are provided to take into account the non-uniform grids and they can be also applied to non-rectangular domains since they are point-wise relations. The proposed technique was studied in several scenarios including homogeneous and inhomogeneous axial and non-axial anisotropic media. It was revealed that for specific ranges of the permittivities and unit cell aspect ratios, the interface yields the most stringent CFL time step across the entire anisotropic domain, which is not predicted by the von-Neumann criterion. However, in isotropic media, the CFL conditions offered by the interfaces are always more relaxed than the CFL conditions of the surrounding media. Several proof cases were demonstrated to verify the theory including homogeneous and inhomogeneous cylinders embedded in the free space sampled by adaptive grids. The validations were performed utilizing the eigenvalue analysis and time-domain simulations. For future works, we are working to generalize the proposed technique to dispersive media. Also, it is interesting to apply the Gershgorin theorem to a PML-enclosed medium. Another suggestion is to investigate the stability behavior of the unconditionally stable FDTD methods in the presence of the boundaries and interfaces using the Gershgorin theorem.

Appendix

The coefficients of the wave equation (22) are given by

$$C_0 = 2 - \left(C_x^+ + C_x^- + C_y^+ + C_y^-\right), \tag{A1}$$

where

$$C_x^+ = \frac{\Delta t^2}{\mu}\left[\frac{\kappa_{yy}(i+1/2,j)}{\Delta x^2} - \frac{\kappa_{xy}(i,j+1/2) - \kappa_{xy}(i,j-1/2)}{2\Delta x \Delta y}\right] = \frac{\Delta t^2}{\mu} D_x^+, \tag{A2}$$

$$C_x^- = \frac{\Delta t^2}{\mu}\left[\frac{\kappa_{yy}(i-1/2,j)}{\Delta x^2} + \frac{\kappa_{xy}(i,j+1/2) - \kappa_{xy}(i,j-1/2)}{2\Delta x \Delta y}\right] = \frac{\Delta t^2}{\mu} D_x^-, \tag{A3}$$

$$C_y^+ = \frac{\Delta t^2}{\mu}\left[\frac{\kappa_{xx}(i,j+1/2)}{\Delta y^2} - \frac{\kappa_{yx}(i+1/2,j) - \kappa_{yx}(i-1/2,j)}{2\Delta x \Delta y}\right] = \frac{\Delta t^2}{\mu} D_y^+, \tag{A4}$$

$$C_y^- = \frac{\Delta t^2}{\mu}\left[\frac{\kappa_{xx}(i,j-1/2)}{\Delta y^2} + \frac{\kappa_{yx}(i+1/2,j) - \kappa_{yx}(i-1/2,j)}{2\Delta x \Delta y}\right] = \frac{\Delta t^2}{\mu} D_y^-, \tag{A5}$$

and also

$$C_1 = \frac{\Delta t^2}{\mu}\left[\frac{\kappa_{xy}(i,j+1/2) + \kappa_{xy}(i,j-1/2) + \kappa_{yx}(i+1/2,j) + \kappa_{yx}(i-1/2,j)}{8\Delta x \Delta y}\right] = \frac{\Delta t^2}{\mu} D_1. \tag{A6}$$

Intellectual Property

The authors confirm that they have given due consideration to the protection of intellectual property associated with this work and that there are no impediments to publication, including the timing of publication, with respect to intellectual property.

Funding

No funding was received for this work.

CRediT Authorship Contribution Statement

K. Hosseini: Idea & conceptualization, Research & investigation, Analysis, Methodology, Software and simulation, Original draft preparation.

Declaration of Competing Interest

The authors hereby confirm that the submitted manuscript is an original work and has not been published so far, is not under consideration for publication by any other journal and will not be submitted to any other journal until the decision will be made by this journal. All authors have approved the manuscript and agree with its submission to "Iranian Journal of Electrical and Electronic Engineering".

References

[1] A. Romano and R. Cavaliere, "Introduction to optics in anisotropic media," in *Geometric Optics*, Vol. 3, Switzerland: Springer, pp. 265–271, 2016.

[2] K. Zhang and D. Li, "Electromagnetic waves in dispersive media and anisotropic media," in *Electromagnetic Theory for Microwaves and Optoelectronics*, 2nd ed., Berlin: Springer, pp. 475–576, 2008.

[3] A. Eroglu, "Microwave devices using anisotropic and gyrotropic media," in *Wave Propagation and Radiation in Gyrotropic and Anisotropic Media*, Switzerland: Springer, pp. 169–215, 2010.

[4] V. Kamra and A. Dreher, "Efficient analysis of multiple microstrip transmission lines with anisotropic substrates," *IEEE Microwave and Wireless Components Letters*, Vol. 28, No. 8, pp. 636–638, Aug. 2018.

[5] J. Lee and D. F. Sievenpiper, "Patterning technique for generating arbitrary anisotropic impedance surfaces," *IEEE Transactions on Antennas and Propagation*, Vol. 64, No. 11, pp. 4725–4732, Nov. 2016.

[6] K. Ichikawa, Z. Zhang, Y. Tsuji, and M. Eguchi, "A single-polarization holey fiber with anisotropic lattice of circular air holes," *Journal of Lightwave Technology*, Vol. 33, No. 18, pp. 3866–3871, Sep. 2015.

[7] T. Touvinen, E. T. Salonen, and M. Berg, "An artificially anisotropic antenna substrate for the generation of circular polarization," *IEEE Transactions on Antennas and Propagation*, Vol. 64, No. 11, pp. 4937–4942, Nov. 2016.

[8] H. Zhihui, L. Hua, and Z. Jianlin, "Polarization independent and non-reciprocal absorption in multi-layer anisotropic black phosphorous metamaterials," *Optics Express*, Vol. 29, No. 14, pp. 21336–21347, Jul. 2021.

[9] K. Yee, "Numerical solution of initial boundary value problems involving Maxwell's equations in isotropic media," *IEEE Transactions on Antennas and Propagation*, Vol. 14, No. 3, pp. 302–307, May 1966.

[10] G. Singh, E. L. Tan, and Z. N. Chen, "A split-step FDTD method for 3-D Maxwell's equations in general anisotropic media," *IEEE Transactions on Antennas and Propagation*, Vol. 58, No. 11, pp. 3647–3657, Nov. 2010.

[11] A. Taflove and S. C. Hagness, *Computational electrodynamics: The finite difference time domain method*. MA, USA: Artech House, 2005.

[12] L. Zhou, F. Yang, J. Ouyang, P. Yang, and R. Long, "ADI scheme of a nonstandard FDTD method and its numerical properties," *IEEE Transactions on Antennas and Propagation*, Vol. 64, No. 10, pp. 4365–4373, Oct. 2016.

[13] A. K. Saxena and K. V. Srivastava, "Higher order LOD-FDTD methods and their numerical dispersion properties," *IEEE Transactions on Antennas and Propagation*, Vol. 65, No. 3, pp. 1480–1485, Mar. 2017.

[14] J. A. Pereda, L. A. Vielva, A. Vegas, and A. Prieto, "Analyzing the stability of the FDTD technique by combining the von Neumann method with the Routh-Hurwitz criterion," *IEEE Transactions on Microwave Theory and Techniques*, Vol. 49, No. 2, pp. 377–381, Feb. 2001.

[15] O. Ramadan, "Stability-improved ADE-FDTD implementation of Drude dispersive models," *IEEE Antennas and Wireless Propagation Letters*, Vol. 17, No. 5, pp. 877–880, May 2018.

[16] H. Choi, J. W. Baek, and K. Y. Jung, "Numerical stability and accuracy of CCPR-FDTD for dispersive medi," *IEEE Transactions on Antennas and Propagation*, Vol. 68, No. 11, pp. 7717–7720, Nov. 2020.

[17] J. Park and K. Y. Jung, "Numerical stability of modified Lorentz FDTD unified from various dispersion models," *Optics Express*, Vol. 29, No. 14, pp. 21639–21654, Jul. 2021.

[18] D. Y. Heh and E. L. Tan, "Generalized stability criterion of 3-D FDTD schemes for doubly lossy media," *IEEE Transactions on Antennas and Propagation*, Vol. 58, No. 4, pp. 1421–1425, Apr. 2010.

[19] D. Y. Heh and E. L. Tan, "Multiple LOD-FDTD method for inhomogeneous coupled transmission lines and stability analyses," *IEEE Transactions on Antennas and Propagation*, Vol. 68, No. 3, pp. 2198–2205, Mar. 2020.

[20] F. Kung and H. T. Chuah, "Stability of classical finite-difference time-domain (FDTD) formulation with nonlinear elements – A new perspective," *Progress In Electromagnetics Research*, Vol. 42, pp. 49–89, 2003.

[21] B. Denecker, L. Knockaert, F. Olyslager, and D. D. Zutter, "A new state-space-based algorithm to assess the stability of finite-difference time-domain method for 3D finite inhomogeneous problems," *International Journal of Electronics and Communications*, Vol. 58, No. 5, pp. 339–348, 2004.

[22] C. T. Schroder and W. R. Scott, "On the stability of the FDTD algorithm for elastic media at a material interface," *IEEE Transactions on Geoscience and Remote Sensing*, Vol. 40, No. 2, pp. 474–481, Feb. 2002.

[23] K. Hosseini and Z. Atlasbaf, "Simple intuitive relations concerning the effect of boundaries on the stability of the FDTD method," *IEEE Transactions on Antennas and Propagation*, Vol. 66, No. 12, pp. 7483–7487, Dec. 2018.

[24] F. Moharrami and Z. Atlasbaf, "Stability analysis of the SBC modeling of graphene in the FDTD method," *IEEE Transactions on Antennas and Propagation*, Vol. 69, No. 4, pp. 2421–2426, Apr. 2020.

[25] T. I. Kosmanis and T. D. Tsiboukis, "A systematic and topologically stable conformal finite-difference time-domain algorithm for modeling curved dielectric interfaces in three dimensions," *IEEE Transactions on Microwave Theory and Techniques*, Vol. 51, No. 3, pp. 839–847, Mar. 2003.

[26] J. Liu, M. Brio, and J. V. Moloney, "An overlapping Yee finite-difference time-domain method for material interfaces between anisotropic dielectrics and general dispersive or perfect electric conductor media," *International Journal of Numerical Modelling*, Vol. 27, pp. 22–33, Jan. 2014.

[27] R. G. Werner, C. A. Bauer, and J. R. Cary, "A more accurate, stable, FDTD algorithm for electromagnetics in anisotropic dielectrics," *Journal of Computational Physics*, Vol. 255, pp. 436–455, 2013.

[28] F. L. Teixeira and W. C. Chew, "On causality and dynamic stability of perfectly matched layers for FDTD simulations," *IEEE Transactions on Microwave Theory and Techniques*, Vol. 47, No. 6, pp. 775–785, Jun. 1999.

[29] G. D. Smith, *Numerical solution of partial differential equations; finite difference methods*. 2nd ed., NY, USA: Clarendon, 1978.

[30] W. Yu and R. Mittra, "A conformal finite-difference time-domain technique for modeling curved dielectric surfaces," *IEEE Microwave and Wireless Components Letters*, Vol. 11, No. 1, pp. 25–27, Jan. 2001.

K. Hosseini received the B.Sc. degree in Electrical Engineering from the University of Tehran, Iran in 2010, and the M.Sc. and Ph.D. degrees in Telecommunications Engineering from Tarbiat Modares University, Tehran, Iran in 2013 and 2018, respectively. He is now an Assistant Professor with the Department of Electrical Engineering, Faculty of Engineering, University of Kurdistan, Sanandaj, Kurdistan, Iran. His research interests include computational electromagnetics, metasurfaces, and optics.